A Spatiotemporal Water Vapor–Deep Convection Correlation Metric Derived from the Amazon Dense GNSS Meteorological Network

DAVID K. ADAMS

Centro de Ciencias de la Atmósfera, Universidad Nacional Autónoma de México, Mexico City, Mexico

HENRIQUE M. J. BARBOSA

Instituto de Física, Universidade de São Paulo, São Paulo, Brazil

KAREN PATRICIA GAITÁN DE LOS RÍOS

Centro de Ciencias de la Atmósfera, Universidad Nacional Autónoma de México, Mexico City, Mexico

(Manuscript received 12 April 2016, in final form 26 August 2016)

ABSTRACT

Deep atmospheric convection, which covers a large range of spatial scales during its evolution, continues to be a challenge for models to replicate, particularly over land in the tropics. Specifically, the shallow-to-deep convective transition and organization on the mesoscale are often not properly represented in coarse-resolution models. High-resolution models offer insights on physical mechanisms responsible for the shallow-to-deep transition. Model verification, however, at both coarse and high resolution requires validation and, hence, observational metrics, which are lacking in the tropics. Here a straightforward metric derived from the Amazon Dense GNSS Meteorological Network (~100 km × 100 km) is presented based on a spatial correlation decay time scale during convective evolution on the mesoscale. For the shallow-to-deep transition, the correlation decay time scale is shown to be around 3.5 h. This novel result provides a much needed metric from the deep tropics for numerical models to replicate.

1. Introduction

Deep precipitating convection dominates tropical meteorology and climate. Given the spatial and temporal scales over which convection evolves and complex interactions with dynamic and thermodynamic fields, it is a challenging phenomenon to reproduce in numerical models of all resolutions. Coarse-resolution models, where convection is parameterized, have had difficulties replicating the continental diurnal convective cycle as well as convective organization on the mesoscale (Bechtold et al. 2004; Grabowski et al. 2006; Folkins et al. 2014). Oftentimes, high-resolution models have been utilized with the goal of ameliorating the continental (tropics or midlatitudes) diurnal cycle or convective organization deficiencies through improvements in model parameterizations (Rio et al. 2009; Rieck et al. 2014). However, high-resolution modeling studies [cloud-resolving models (CRM) to large-eddy simulation (LES)] have also been employed to infer the actual physical mechanisms responsible for convective development/organization (e.g., cold pools). The shallow-to-deep convective transition (STD transition), which coarser-resolution models often fail to replicate, has received special attention. For example, modeling studies have indicated that cold pool formation (Kuang and Bretherton 2006; Khairoutdinov and Randall 2006; Schlemmer and Hohenegger 2016), increasing cloud buoyancy (Wu et al. 2009), cumulus congestus moistening (Waite and Khouider 2010), or large-scale vertical motions (Hohenegger and Stevens 2013) control the STD transition. Nevertheless, these mechanistic deductions from high-resolution models also require validation with high spatial–temporal resolution observations.

Ascertaining the physical realism of models with domain sizes on the order of 100 km × 100 km requires

Corresponding author address: David K. Adams, Centro de Ciencias de la Atmósfera, Universidad Nacional Autónoma de México, Circuito Exterior s/n, Ciudad Universitaria, Del. Coyoacán 04510 D. F., Mexico City, Mexico.
E-mail: dave.k.adams@gmail.com

DOI: 10.1175/MWR-D-16-0140.1

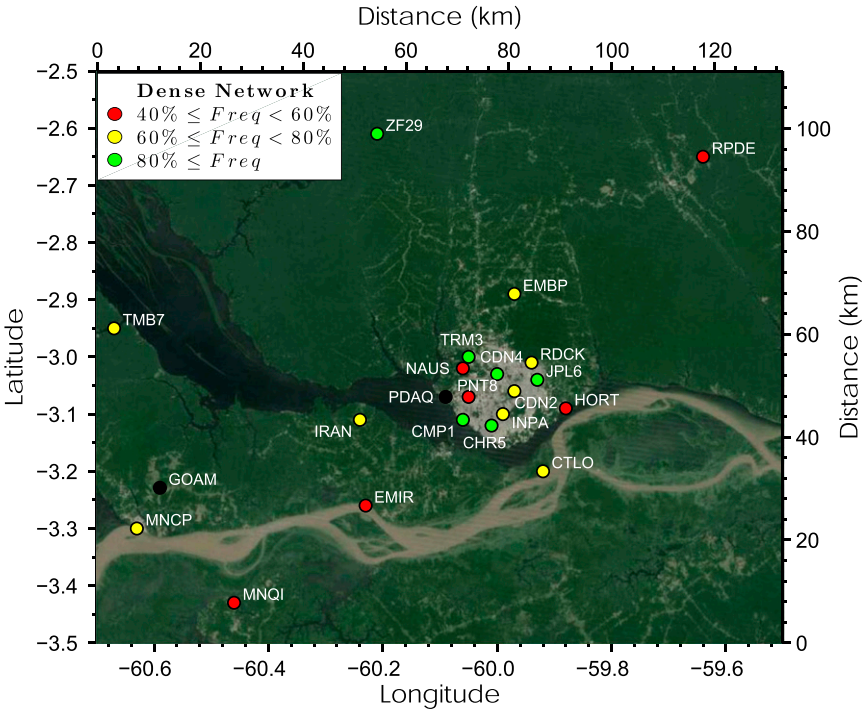

FIG. 1. Map of the Manaus Dense GNSS Meteorological Network from April 2011 to April 2012. The color scheme represents the frequency of PWV data (11 256 total data values) for the 67 convective events used in this study. GOAM data were not utilized. PDAQ failed in October and was not utilized in the PWV anomaly plot (Fig. 4), but was used in correlation vs distance statistics to better assess the data-denial tests.

corresponding mesoscale observations, which are typically lacking in the continental tropics. The Amazon Dense GNSS Meteorological Network (ADGMN) (Adams et al. 2015) was created precisely to investigate mesoscale water vapor–convection interactions, specifically, to examine the STD transition and to test for responsible mechanisms. The ADGMN's high temporal and spatial meteorological data lend themselves to metric creation to validate models, which motivates this present study.

Although cloud-top temperature (CTT) from satellite platforms can be used to evaluate cloud evolution (e.g., Hohenegger and Stevens 2013), metrics based on Global Navigational Satellite Systems (GNSS)/global positioning system (GPS) precipitable water vapor (PWV) are advantageous for several reasons. First, GNSS PWV frequency (≈5 min) provides sufficient temporal resolution for rapidly developing cumulus fields. Moreover, GNSS PWV is all-weather accurate, including cloudy and rainy conditions associated with deep convection. Furthermore, PWV has a strong relationship with tropical convective precipitation and has served as the critical variable in numerous studies relating tropical convection to thermodynamics (Raymond 2000; Bretherton et al. 2004; Lintner et al. 2011; Hottovy and Stechmann 2015; Schiro et al. 2016). Finally, in models, PWV is a trivial variable to calculate unlike variables derived from cloud microphysical parameterizations.

Since mesoscale observationally based metrics are in short supply in the tropics, we propose a novel metric based on spatial cross correlations for gauging the mesoscale spatiotemporal evolution of Amazonian convection. Similar to Adams et al. (2013), who used 3.5 yr of GPS PWV from the Instituto Nacional de Pesquisas da Amazônia (INPA) (see Fig. 1) to derive a "water vapor convergence" time scale, we also focus on the STD transition. Adams et al. (2013) inferred, based on the observed joint evolution of cloud fields and PWV, a characteristic STD transition time scale of ~4 h. Here, the temporal evolution of the spatial correlation of PWV fields is described with an exponential function, providing a spatial correlation decay time scale; a useful diagnostic for models. In what follows, we describe the ADGMN, bring to light some ambiguities associated with the definition of the STD transition, and present the methodology for analyzing spatial correlation decay time scales. Results focused on the seasonal and, particularly, the diurnal cycle are presented. Remarks on

future studies with ADGMN data and expanding GNSS meteorological networks in the tropics conclude the paper.

2. Context and motivation, study site, data, and methodology

a. Context and motivation

In its most generic form, the STD transition can be idealized as the process of shallow cumulus, growing into cumulus congestus, perhaps with showers, and finally morphing into deep precipitating convective towers on typical time scales of 2–4 h (Wu et al. 2009; Hohenegger and Stevens 2013; Adams et al. 2013). However, perusal of the literature reveals rather varied, and somewhat ambiguous, usage of the STD transition concept, potentially leading to confusion. To contextualize the present study and clarify the intended usage of our derived metric, we divide STD transition studies into three categories. These categories are neither exhaustive nor necessarily mutually exclusive, though certainly nearly all studies could fit comfortably within one. The first category, under which our study falls, follows Zehnder et al. (2006), Zhang and Klein (2010), and Adams et al. (2013), all observationally based studies of continental convection. Here, a fixed geographical area (<50 km) is observed instrumentally, an Eulerian and decidedly mesoscale perspective, as ''individual'' convective events develop over it. The temporal evolution of these convective events is typically composited to derive transition time scales (Adams et al. 2013) or evaluate thermodynamic or environmental conditions during the transition (Zehnder et al. 2006; Zhang and Klein 2010). A second category, for which our metric is intended, involves high-resolution models. These CRM and LES modeling studies (~100 km × 100 km) probe the complete temporal evolution of deepening cumulus cloud fields over an entire spatial domain. Convective cloud ensembles, during their different phases, provide domain-averaged variables for time-scale analysis and/or for inferring physical controls on the STD transition (e.g., cold pools, a critical lapse rate, congestus moistening, and dynamical lifting) (Khairoutdinov and Randall 2006; Wu et al. 2009; Waite and Khouider 2010; Hohenegger and Stevens 2013). Oftentimes, a single criterion such as domain/ensemble-averaged cloud growth rate (Wu et al. 2009) is employed to signify that the transition has occurred. A third category, often couched or framed in the language of the STD transition, could more accurately be described as suppressed versus convectively active conditions (Sahany et al. 2012; Hagos et al. 2014; Powell and Houze 2015). This category of studies, both modeling (Kuang and Bretherton 2006) and observational (Xu and Rutledge 2016), are representative of much larger-scale circulations and their dynamic and thermodynamic conditions in which cumulus fields transition to deep convection. Their ''shallow-to-deep transition'' takes place on the order of days to greater than one week.

It should also be noted, however, that even the generic definition of three well-defined cumulus modes and their evolution may be overly idealized (Kumar et al. 2013). Consequently, we reserve some flexibility in defining the STD transition, reflecting our approach and intent to create an easily reproducible metric. As noted above, we consider the time evolution of deep convective events at a single site concomitantly with surrounding water vapor fields. We do not discern the thermodynamic or dynamic conditions leading to the transition nor whether the convective event is associated with an already mature propagating mesoscale convective system. Nevertheless, since our metric is derived from CTT temporal evolution (''warm'' >280-K shallow cumulus to ''cold'' <235-K deep cumulonimbus), this ensures some form of STD transition is captured during our convective events (see section 2d).

b. Study site

The central Amazon, in and around Manaus (3.05°S, 60.21°W), represents a tropical rain forest climate with rainfall throughout the year, but with a notable minimum during July and August (Machado et al. 2004). There is a marked diurnal cycle; however, larger-scale synoptic forcing and/or long-lived mesoscale squall lines modulate the convective timing and intensity (Williams et al. 2002). Topographic relief is small (~150 m). Nevertheless, land surface heterogeneity due to river-forest contrast generates favored zones of water vapor convergence (Adams et al. 2015) influencing precipitation timing and intensity (Fitzjarrald et al. 2008).

To derive metrics, long-term mesoscale observational studies of tropical convection are necessary. The mesoscale ADGMN (~100 km × 100 km) was created to study the complex interactions between water vapor and deep convection in a continental equatorial setting (Adams et al. 2015). The ADGMN (Fig. 1) originally consisted of 10 sites, expanding to 21 sites during the last 8 months of the experiment.[1] Because of the inaccessible rain forest or seasonally flooded terrain surrounding Manaus, sites were concentrated in the urban zone.

[1] The GOAmazon (GOAM) site created in anticipation of ARM Mobile Facility deployment (2014–15) had only 4 months of data and was excluded from the present analysis.

Nevertheless, the network spanned the subtle topographic effects, including elevated forest transition sites (EMBP, RDCK, RPDE, TRM3), low-lying rivers sites (CTLO, CMP1, CHR5, EMIR, HORT, MNCP, MNQI, PDAQ, TMB7), as well as a pristine rain forest station (ZF29). Mean station separation is 41 km, the largest (MNCP-RPDE) is 131 km and the smallest (INPA-CHR5), 3.3 km. Station concentration in Manaus implies highly correlated PWV, which is considered in section 2c.

c. Data

Tropical water vapor observations capturing convective evolution are either too infrequent (e.g., radiosondes, polar-orbiting satellites), invalid, or of questionable quality under cloudy/rainy conditions (e.g., vertically pointing microwave radiometers, satellite IR). Condensate and precipitation effects at GNSS microwave frequencies are small (Solheim et al. 1999) and the accuracy of GNSS PWV relative to radiosondes and radiometers (≈1–2 mm) has been well established (Bevis et al. 1992; Rocken et al. 1993). Even in the high humidity, logistically challenging environment of the Amazon, GNSS PWV is accurate (Sapucci et al. 2007; Adams et al. 2011a,b, 2015). The GNSS PWV observation cone (radius ~10 km) and ADGMN site distribution permit capturing PWV field evolution from the cumulus stage to cumulonimbus lines or clusters.

For the 21 stations, GNSS PWV was estimated every 5 min with GPS-Inferred Positioning System and Orbit Analysis Simulation Software (GIPSY-OASIS), utilizing geodetic-grade receivers and antennas and surface pressure and temperature from collocated meteorological sensors. Where meteorological sensors failed or did not exist (only the NAUS site) pressure, using the hypsometric equation, and temperature were interpolated from the nearest station. The region's homogeneous temperature fields and flat topography ensure this interpolation has negligible effects on PWV.

To identify deep convective events, INPA surface precipitation as well as *GOES-12* (10.7 μm) satellite data were employed. Since INPA failed at the end of 2011, Tropical Rainfall Measuring Mission (TRMM) 3B42 (3-h precipitation rate) from the 25 km × 25 km pixel centered over CHR5, the closest station, was used. *GOES-12* IR brightness temperature (i.e., CCT) was calculated as the average of the 4 × 4 pixels (16 km × 16 km) corresponding to the GNSS cone of observation centered over INPA (2011) and over CHR5 (2012).

d. Methodology

For calculating correlation decay time scales during the mesoscale evolution to deep convection, the convective events were identified essentially following Adams et al. (2013). A deep convective event was defined as reporting precipitation and, minimally, a 50-K fall in CTT in less than 2 h to 235 K or below. This definition results in minimizing misidentification of stratiform and showery congestus precipitation as deep convective precipitation as well as ensuring that a shallow cumulus stage is observed. Likewise, these strong CTT drops were associated with large upswings in PWV, the peak of which was utilized as the temporal identifier of the convective event origin (i.e., $t = 0$). The time series of the correlation versus distance slope, based on each time bin, was then extended backward 14 h prior to time of maximum PWV, as in Adams et al. (2013). This implies covering the entire diurnal cycle, though here we focus solely on the last 6 h, which contains the STD transition. Over the 1-yr period of study, 118 days reported some form of precipitation; however, only 67 deep convective events met these more stringent criteria.

To quantify the spatiotemporal evolution of PWV, cross correlations between stations were calculated in 30-min and 1-h bins. Each time bin correlation was calculated from $t = 0$ h (i.e., convective event occurrence) every hour or every 30 min. For example, in the first hour with respect to convective event occurrence; that is, between $t = 0$ and $t = -1$ h, there are 12 total 5-min PWV values for each individual event. Given 67 convective events, this would then imply a maximum of $12 \times 67 = 804$ data points within that 1-h time bin to be correlated with the corresponding $t = 0$ to $t = -1$ h data points from a different station. This is then carried out for every time bin, $t = -1$ to $t = -2$ h, . . . , up to $t = -13$ to $t = -14$ h. With up to 20 other stations available for cross correlation in the corresponding 1-h time bin, as many as 231 correlation coefficients enter into the calculation of the separation distance versus correlation coefficient. In this way, the slope of correlation coefficient versus distance, for each 1-h bin, was estimated (significant to the 95th percentile) from the fitted regression line fixed at correlation coefficient $R = 1$ at distance $x = 0$ (see Fig. 2). The change in slope of these fitted regression lines, as a function of time, is then evaluated. The resulting temporal evolution of spatial correlation is described by a simple functional form from which a time decay constant is derived, thereby providing an easily replicable metric.

Taking into account the network's irregular geographical configuration, the time evolution of the cross correlations was checked for sensitivity to this spatial distribution in two ways. First, as a direct approach, five closely spaced and centrally located stations (PDAQ, PNT8, RDCK, INPA, and NAUS) were

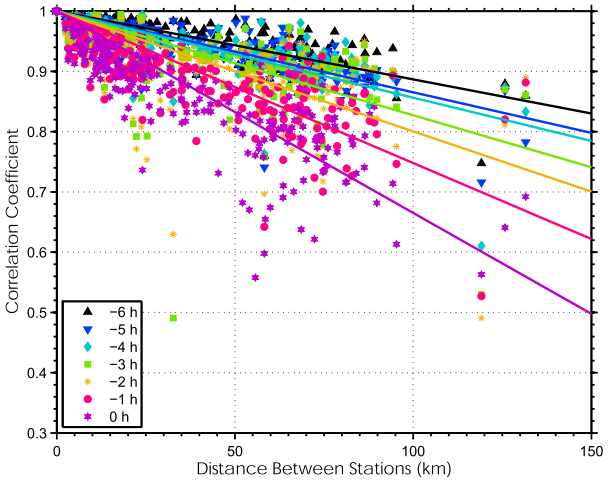

FIG. 2. Scatterplot of correlation vs separation distance as a function of different 1-h time bins, between $t = 0$ and $t = -6$ h for the 67 events. The slope of the fitted lines is statistically significant at the 95th percentile.

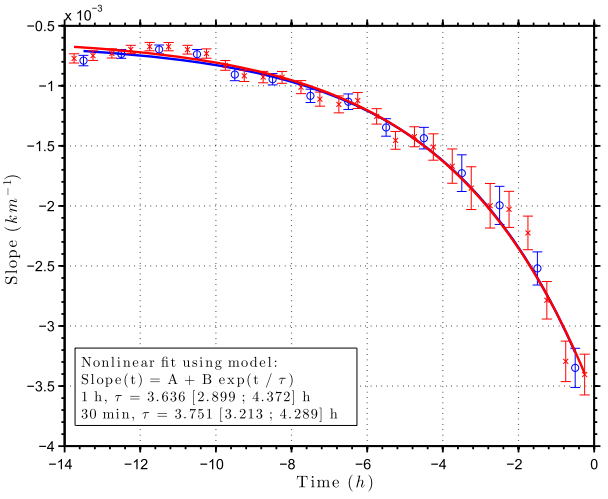

FIG. 3. Temporal evolution of correlation vs separation distance slope with exponential fit and error bars for 67 convective events. Both 1-h (blue lines and circles) and 30-min (red line and × symbols) time bins are included for comparison purposes. Functional form, average decay time scale, τ, and 95th percentile confidence intervals are shown.

removed and the calculations repeated. The average station separation distance rose from 41 to 53 km, diminishing the influence of these highly correlated stations. Second, we implemented a Monte Carlo approach in which one station was randomly removed and the data resampled. The correlation slope with distance for each time bin was recalculated for 100 trials. The time constant from the fitted function and its associated uncertainties were evaluated for the 100 trials, and this was performed as 2 through 18 stations were removed (see section 3).

Considering that varying conditions (e.g., surface forcing or free-tropospheric thermodynamic structure) may influence the correlation decay time scale, drier (July–December) versus wet season (January–April), as well as the diurnal cycle of convection, were examined. We provide more details on the latter in section 3, given that the continental diurnal cycle and specifically from the Amazon region (Betts and Jakob 2002a,b; Grabowski et al. 2006, among many others) underpins much of the original STD transition research; in addition to our goal of providing an easily replicable metric.

3. Results and discussion

The 67 convective events occurred mostly following the diurnal cycle (55 events) with two-thirds occurring between 1200 and 1800 local time (LT) (44 events). ''Nocturnal'' convection (2000 LT through 1200 LT the following day) consisted of only 12 events. For the purpose of seasonal comparison, the wet season consisted of 24 events while the drier seasons consisted of 27 without consideration for the time of occurrence. The 16 events occurring between April and July 2011 were not included in the seasonal comparison since only 10 GNSS meteorological sites existed at that time.

Figure 2 displays the correlation coefficient as a function of distance for 1-h time bins over the 67 convective events. For visual clarity, and to focus on the STD transition, only the 6 h prior ($t = -6$ to $t = 0$ h) to the convective event are displayed. This figure represents the time evolution of spatial correlations; that is, the change in angle between the slopes for each time bin represents the temporal evolution of spatial decorrelation. The lines fitted to the correlation versus station separation distance are fixed to $R = 1$ at $x = 0$. Although scatter is large, the slopes calculated are all statistically significant (95th percentile). As one considers progressively earlier times before the development of convective activity (prior to $t = -6$ h), the fitted lines fall closely one upon the other (not shown), and correlation decays only slightly (~0.15) over the maximum separation distance of the network. Within $t = 0$ h, correlation decays rapidly to ~0.5 at the limit of separation distance (~150 km). When these slopes are expressed as a function of time, the functional form becomes apparent (Fig. 3). From the analysis of these 67 events, there is a nonlinear decay in correlation beginning around $t = -4$ h and only a weaker quasi-linear decay back to $t = -12$ h (Fig. 3). In this figure, both 1-h and 30-min bins data are plotted making clear that this temporal binning is unimportant. The error

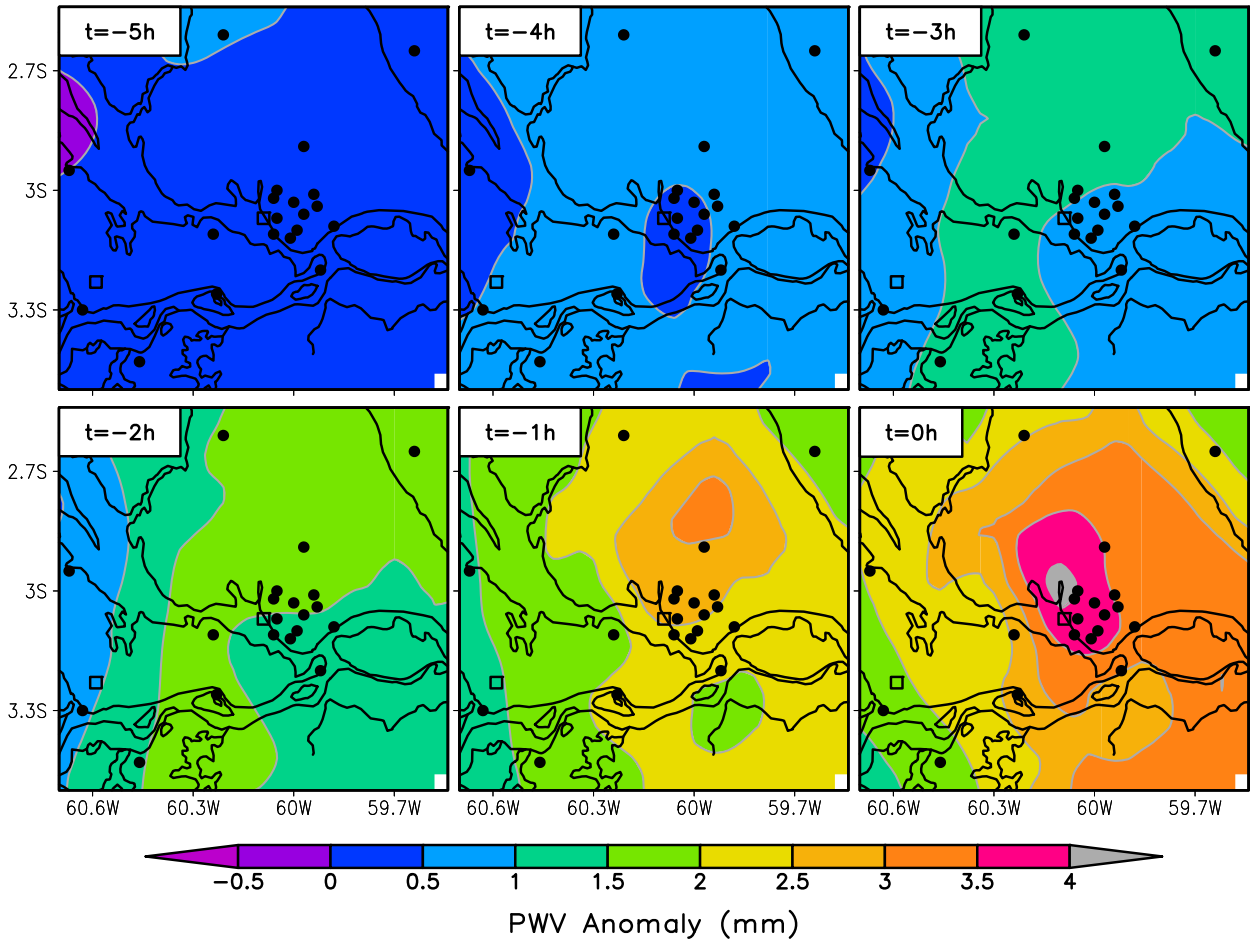

FIG. 4. Plot of PWV anomalies (mm) fields calculated from the average of 67 convective events for the 5 h before convective events.

bars represent the 95th percentile range for the correlation versus distance coefficients used to derive the slope (i.e., the lines in Fig. 2). Fitted with an exponential function, a correlation decay time scale of ~3.5 h is revealed.

Solely for visualization purposes, PWV anomaly fields from $t = -5$ to $t = 0$ h are shown in Fig. 4. Anomalies were calculated by subtracting the average (over all stations and all times) from the 1-h bin average of the 67 events at each site. Cressman interpolation analysis was utilized for plotting; the plots being fairly insensitive to the radius of influence chosen. The PWV anomaly fields are fairly flat from $t = -5$ to $t = -4$ h. Commencing at $t = -3$ h, the water vapor fields become more structured, maximizing the PWV anomaly gradient, and concentrating the positive PWV anomalies (i.e., a proxy for water vapor convergence) in the central portion of the network. Given that the initiation of deep convection is associated with the largest positive PWV anomalies at INPA (2011) and CHR5 (2012), a maximum positive PWV anomaly centered near INPA, or nearby, should be expected. Similar results are obtained, not surprisingly, for CTT (as shown in the example for the 55 diurnal convective events in Fig. 7).

To test the decay time-scale robustness, data denial analyses were carried out. In the first case, the five clustered stations noted in section 2c were removed directly and statistics recalculated. The results are essentially identical with mean $\tau = 3.45$ h and $\sigma = 0.362$ h. For the Monte Carlo random data denial analysis, the elimination of 10 sites produces a mean difference of −0.1 h and an increase in σ of 0.21 to $\sigma = 0.57$ h, indicating minimal influence of the station distribution.

Decay time-scale sensitivity to environmental conditions was gauged through analysis of wet season versus the dry and dry-to-wet transition season as well as diurnal versus nocturnal convective events (Figs. 5 and 6). Thermodynamic conditions, in particular stability measures, (e.g., CAPE, CIN) as well as the water vapor distribution vary seasonally in the Amazon, influencing

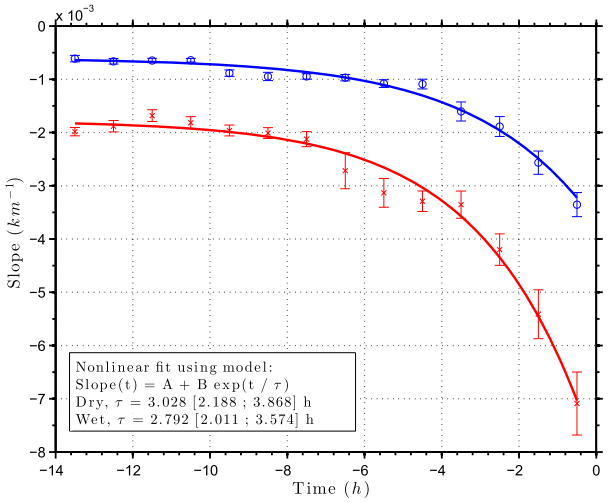

FIG. 5. Temporal evolution of correlation vs separation distance slope with exponential fit and error bars for wet (red, 24 events) and dry and dry-to-wet season (blue, 27 events). The 16 events occurring during the wet-to-dry transition are not included.

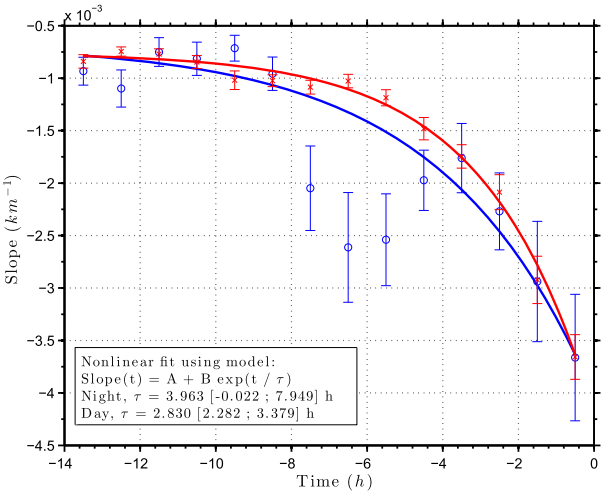

FIG. 6. Temporal evolution of correlation vs separation distance slope with exponential fit and error bars for diurnal (55 events, red) and nighttime (12 events, blue).

the intensity and frequency of convection (Fu et al. 1999; Li and Fu 2004). The dry and dry-to-wet transition experience less frequent, but often more intense convection (Williams et al. 2002). During the wet season, precipitating convection is frequent and the free troposphere approaches a moist adiabat tied to the subcloud layer, thereby limiting both CAPE and CIN, but increasing precipitation efficiency (Machado et al. 2004). Figure 5 contains a comparison of decay time scales associated with the 24 wet and 27 dry/dry-to-wet season convective events. The wet season demonstrates much greater heterogeneity, with larger decreases in spatial correlations compared to dry/dry-to-wet seasons. Visual inspection of GOES CTT animations also shows widerspread cumulus convection typically deepening and organizing over different portions of the network during the wet season. Though wet season spatial correlation scales are much smaller, the decay time scale are essentially the same; $\tau = 2.72$ h (wet) and $\tau = 3.02$ h (dry/dry to wet).

Considering that the continental tropical diurnal cycle has strongly motivated the research of the STD transition, we have examined diurnal versus nocturnal convection. From Fig. 6, the decay time scale increases by approximately 1 h, $\tau = 2.83$ h (diurnal), and $\tau = 3.96$ h (nocturnal). The nocturnal evolution deviates strongly from the exponential fit around $t = -8$ to $t = -6$ h, but still displays the correlation drop off during the STD transition; that is, the last 4 h prior to deep convection (Adams et al. 2013). Examination of GOES CTT animations reveals no obvious deviating behavior 8–6 h prior to $t = 0$ for these nocturnal events. Nonetheless, with only 12 events, these statistics are certainly less reliable. To confirm that the STD transition, as most commonly studied, is occurring, composites of CTT were also created for the diurnal convective events. In Fig. 7, the composite CTT fields of the 55 diurnal events are presented. Prior to $t = -3$ h, the CTT fields are homogeneous. Between $t = -3$ h and the convective event ($t = 0$), cloud fields begin to deepen rapidly (i.e., the STD transition).

The decay time scale derived from the above analysis is consistent with the 4-h water vapor convergence time scale for the Amazon STD transition (Adams et al. 2013). This provides for a physical interpretation. Consider the simplest case of the 55 diurnal convective events. The 10-km-radius GPS cone of view observes cumulus clouds interspersed with clear sky during the shallow phase. With solar insolation, convective boundary layer deepening and cumulus cloud growth result in $d(\mathrm{PWV})/dt > 0$ (a proxy for water vapor convergence in the atmospheric column). At this stage, all sites in the network essentially behave the same and PWV time evolution is correlated over greater distances. As congestus clouds grow, convergence zones begin to narrow. Figures 5 and 6 of Khairoutdinov and Randall (2006) provide a nice visualization of this process (which they attribute to cold pool collisions). Simultaneously, water vapor convergence weakens over the ''noncongestus regions'' and spatial decorrelation increases. Finally, growth into deep cumulonimbus towers, lines, and clusters with stronger vertical accelerations confines the zones of augmenting $d(\mathrm{PWV})/dt > 0$ even more so, and the rest of the network experiences much weaker, zero water vapor convergence or

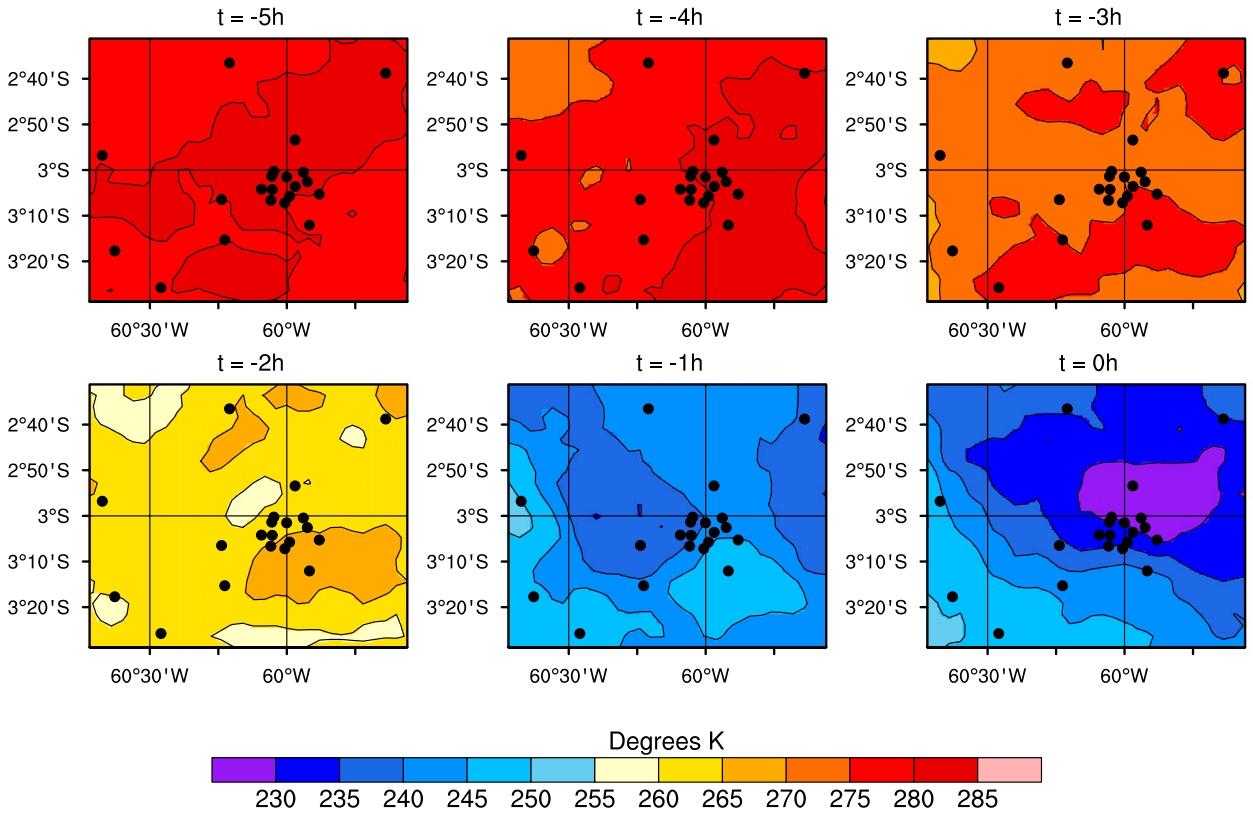

FIG. 7. Plot of the temporal evolution ($t = -5$ to $t = 0$ h) of GOES cloud-top temperature (K) fields calculated for 55 diurnal convective events.

perhaps even divergence. This deep convective stage further accelerates the decorrelation. Examining Figs. 4 and 7, one can idealize the decorrelation length scale as the inverse of the probability of a station lying within the same contours as other stations. This probability decreases as t approaches 0 h (i.e., more contours on the figures). The spatial structuring (i.e., decreased correlation length) and intensity of water vapor convergence are thus intrinsically tied together and, hence, is a useful gauge of the STD transition. One could certainly speculate that growth into mesoscale convective systems again increases PWV correlation length given induced mesoscale circulations and associated water vapor convergence fields, but this will be investigated in another study.

4. Conclusions and future work

This derived correlation decay time scale is agnostic with respect to any of the putative physical mechanisms responsible for the STD transition. Nevertheless, for at least the case of continental tropical convection, high-resolution models making mechanistic deductions with respect to convective evolution can now attempt to replicate this metric. In future work, ADGMN data will be employed to examine the possible role of cold pools in the STD transition, correlating their occurrence with the increase in water vapor convergence and observed cloud growth. Fortunately, in recent years, GNSS/GPS meteorology has expanded into tropical regions, Continuously Operating Caribbean GPS Observational Network (COCONet) in the Caribbean and Trans-boundary, Land and Atmosphere Long-term Observational and Collaborative Network (TLALOCNet) in Mexico. The large-scale networks provide many anchor sites around which mesoscale dense network can be created in varying topographic and climatic settings.

Acknowledgments. We thank Ben Lintner and Yolande Serra for their comments on the manuscript. We also thank Alain Protat and two anonymous reviewers for their constructive criticisms. Financial support for the ADGMN came through Cooperation Project 0050.0045370.08.4 between PETROBRAS and INPE (Brazil) and from the INPA/LBA (Brazil) (Principle Investigator Icaro Vitorello). H. B. acknowledges the financial support of FAPESP Grant 2013/50510-5. Financial support for this paper was also provided by UNAM PAPIIT IA100916. We also thank the students

of the graduate program Clima e Ambiente (UEA/INPA) for their contributions. Data are available upon request from the corresponding author.

REFERENCES

Adams, D. K., R. M. S. Fernandes, and J. M. F. Maia, 2011a: GNSS precipitable water vapor from an Amazonian rain forest flux tower. *J. Atmos. Oceanic Technol.*, **28**, 1192–1198, doi:10.1175/JTECH-D-11-00082.1.

——, and Coauthors, 2011b: A dense GNSS meteorological network for observing deep convection in the Amazon. *Atmos. Sci. Lett.*, **12**, 207–212, doi:10.1002/asl.312.

——, S. I. Gutman, K. L. Holub, and D. S. Pereira, 2013: GNSS observations of deep convective time scales in the Amazon. *Geophys. Res. Lett.*, **40**, 2818–2823, doi:10.1002/grl.50573.

——, and Coauthors, 2015: The Amazon dense GNSS meteorological network: A new approach for examining water vapor and deep convection interactions in the tropics. *Bull. Amer. Meteor. Soc.*, **96**, 2151–2165, doi:10.1175/BAMS-D-13-00171.1.

Bechtold, P., J. Chaboureau, A. Beljaars, A. Betts, M. Kohler, M. Miller, and J. Redelsperger, 2004: The simulation of the diurnal cycle of convective precipitation over land in a global model. *Quart. J. Roy. Meteor. Soc.*, **130**, 3119–3137, doi:10.1256/qj.03.103.

Betts, A. K., and C. Jakob, 2002a: Evaluation of the diurnal cycle of precipitation, surface thermodynamics, and surface fluxes in the ECMWF model using LBA data. *J. Geophys. Res.*, **107**, doi:10.1029/2001JD000427.

——, and ——, 2002b: Study of diurnal cycle of convective precipitation over Amazonia using a single column model. *J. Geophys. Res.*, **107**, 4732, doi:10.1029/2002JD002264.

Bevis, M., S. Businger, T. A. Herring, C. Rocken, R. Anthes, and R. H. Ware, 1992: GPS meteorology: Sensing of atmospheric water vapor using the Global Positioning System. *J. Geophys. Res.*, **97**, 15 787–15 801, doi:10.1029/92JD01517.

Bretherton, C. S., M. E. Peters, and L. E. Back, 2004: Relationships between water vapor path and precipitation over the tropical oceans. *J. Climate*, **17**, 1517–1528, doi:10.1175/1520-0442(2004)017<1517:RBWVPA>2.0.CO;2.

Fitzjarrald, D. R., R. K. Sakai, O. L. L. Moraes, R. C. de Oliveira, O. C. Acevedo, M. J. Czikowsky, and T. Beldini, 2008: Spatial and temporal rainfall variability near the Amazon-Tapajós confluence. *J. Geophys. Res.*, **113**, G00B11, doi:10.1029/2007JG000596.

Folkins, I., T. Mitovski, and J. R. Pierce, 2014: A simple way to improve the diurnal cycle in convective rainfall over land in climate models. *J. Geophys. Res. Atmos.*, **119**, 2113–2130, doi:10.1002/2013JD020149.

Fu, R., B. Zhu, and R. E. Dickinson, 1999: How do atmosphere and land surface influence seasonal changes of convection in the tropical Amazon? *J. Climate*, **12**, 1306–1321, doi:10.1175/1520-0442(1999)012<1306:HDAALS>2.0.CO;2.

Grabowski, W. W., and Coauthors, 2006: Daytime convective development over land: A model intercomparison based on LBA observations. *Quart. J. Roy. Meteor. Soc.*, **132**, 317–344, doi:10.1256/qj.04.147.

Hagos, S., Z. Feng, K. Landu, and C. N. Long, 2014: Advection, moistening, and shallow-to-deep convection transitions during the initiation and propagation of Madden-Julian Oscillation. *J. Adv. Model. Earth Syst.*, **6**, 938–949, doi:10.1002/2014MS000335.

Hohenegger, C., and B. Stevens, 2013: Preconditioning deep convection with cumulus convection. *J. Atmos. Sci.*, **70**, 448–464, doi:10.1175/JAS-D-12-089.1.

Hottovy, S., and S. N. Stechmann, 2015: A spatiotemporal stochastic model for tropical precipitation and water vapor dynamics. *J. Atmos. Sci.*, **72**, 4721–4738, doi:10.1175/JAS-D-15-0119.1.

Khairoutdinov, M., and D. Randall, 2006: High-resolution simulation of shallow-to-deep convection transition over land. *J. Atmos. Sci.*, **63**, 3421–3436, doi:10.1175/JAS3810.1.

Kuang, Z., and C. S. Bretherton, 2006: A mass-flux scheme view of a high-resolution simulation of a transition from shallow to deep cumulus convection. *J. Atmos. Sci.*, **63**, 1895–1909, doi:10.1175/JAS3723.1.

Kumar, V., C. Jakob, A. Protat, P. T. May, and L. Davies, 2013: The four cumulus cloud modes and their progression during rainfall events: A C-band polarimetric radar perspective. *J. Geophys. Res. Atmos.*, **118**, 8375–8389, doi:10.1002/jgrd.50640.

Li, W., and R. Fu, 2004: Transition of the large-scale atmospheric and land surface conditions from the dry to the wet season over Amazonia as diagnosed by the ECMWF Re-Analysis. *J. Climate*, **17**, 2637–2651, doi:10.1175/1520-0442(2004)017<2637:TOTLAA>2.0.CO;2.

Lintner, B. R., C. E. Holloway, and J. D. Neelin, 2011: Column water vapor statistics and their relationship to deep convection, vertical and horizontal circulation, and moisture structure at Nauru. *J. Climate*, **24**, 5454–5466, doi:10.1175/JCLI-D-10-05015.1.

Machado, L. A. T., H. Laurent, N. Dessay, and I. Miranda, 2004: Seasonal and diurnal variability of convection over the Amazonia: A comparison of different vegetation types and large scale forcing. *Theor. Appl. Climatol.*, **78**, 61–77, doi:10.1007/s00704-004-0044-9.

Powell, S. W., and R. A. Houze Jr., 2015: Evolution of precipitation and convective echo top heights observed by TRMM radar over the Indian Ocean during DYNAMO. *J. Geophys. Res. Atmos.*, **120**, 3906–3919, doi:10.1002/2014JD022934.

Raymond, D., 2000: Thermodynamic control of tropical rainfall. *Quart. J. Roy. Meteor. Soc.*, **126**, 889–898, doi:10.1002/qj.49712656406.

Rieck, M., C. Hohenegger, and C. C. van Heerwaarden, 2014: The influence of land surface heterogeneities on cloud size development. *Mon. Wea. Rev.*, **142**, 3830–3846, doi:10.1175/MWR-D-13-00354.1.

Rio, C., F. Hourdin, J.-Y. Grandpeix, and J.-P. Lafore, 2009: Shifting the diurnal cycle of parameterized deep convection over land. *Geophys. Res. Lett.*, **36**, L07809, doi:10.1029/2008GL036779.

Rocken, C., R. H. Ware, T. V. Hove, F. Solheim, C. Alber, J. Johnson, M. Bevis, and S. Businger, 1993: Sensing atmospheric water vapor with the Global Positioning System. *Geophys. Res. Lett.*, **20**, 2631–2634, doi:10.1029/93GL02935.

Sahany, S., J. D. Neelin, K. Hales, and R. B. Neale, 2012: Temperature–moisture dependence of the deep convective transition as a constraint on entrainment in climate models. *J. Atmos. Sci.*, **69**, 1340–1358, doi:10.1175/JAS-D-11-0164.1.

Sapucci, L. F., L. A. T. Machado, J. F. G. Monico, and A. Plana-Fattori, 2007: Intercomparison of integrated water vapor

estimates from multisensors in the Amazonian region. *J. Atmos. Oceanic Technol.*, **24**, 1880–1894, doi:10.1175/JTECH2090.1.

Schiro, K. A., J. D. Neelin, D. K. Adams, and B. R. Lintner, 2016: Deep convection and column water vapor over tropical land versus tropical ocean: A comparison between the Amazon and the tropical western Pacific. *J. Atmos. Sci.*, **73**, 4043–4063, doi:10.1175/JAS-D-16-0119.1.

Schlemmer, L., and C. Hohenegger, 2016: Modifications of the atmospheric moisture field as a result of cold-pool dynamics. *Quart. J. Roy. Meteor. Soc.*, **142**, 30–42, doi:10.1002/qj.2625.

Solheim, F., J. Vivekanandan, R. H. Ware, and C. Rocken, 1999: Propagation delays induced in GPS signals by dry air, water vapor, hydrometeors, and other particulates. *J. Geophys. Res.*, **104**, 9663–9670, doi:10.1029/1999JD900095.

Waite, M. L., and B. Khouider, 2010: The deepening of tropical convection by congestus preconditioning. *J. Atmos. Sci.*, **67**, 2601–2615, doi:10.1175/2010JAS3357.1.

Williams, E., and Coauthors, 2002: Contrasting convective regimes over the Amazon: Implications for cloud electrification. *J. Geophys. Res.*, **107**, 8082, doi:10.1029/2001JD000380.

Wu, C.-M., B. Stevens, and A. Arakawa, 2009: What controls the transition from shallow to deep convection? *J. Atmos. Sci.*, **66**, 1793–1806, doi:10.1175/2008JAS2945.1.

Xu, W., and S. Rutledge, 2016: Time scales of shallow-to-deep convective transition associated with the onset of Madden–Julian Oscillations. *Geophys. Res. Lett.*, **43**, 2880–2888, doi:10.1002/2016GL068269.

Zehnder, J., L. Zhang, D. Hansford, A. Radzan, N. Selover, and C. Brown, 2006: Using digital cloud photogrammetry to characterize the onset and transition from shallow to deep convection over orography. *Mon. Wea. Rev.*, **134**, 2527–2546, doi:10.1175/MWR3194.1.

Zhang, Y., and S. A. Klein, 2010: Mechanisms affecting the transition from shallow to deep convection over land: Inferences from observations of the diurnal cycle collected at the ARM Southern Great Plains site. *J. Atmos. Sci.*, **67**, 2943–2959, doi:10.1175/2010JAS3366.1.